Supplementary Information

Biocatalytic cascade combining an engineered pyranose 2-oxidase and transaminases for the synthesis of amino sugars

Litavadee Chuaboon[a,b], Surawit Visitsatthawong [c], Orawan Sookbampen [b], Siripakorn Suthin[b], Moritz Voss [d], Thanyaporn Wongnate [c], Matthias Höhne [e], Uwe T. Bornscheuer [d], Pimchai Chaiyen[* c]

[a] School of Pharmacy, Walailak University, Nakhonsrithammarat 10800, Thailand

[b] Biomass and oil palm center of excellence, Walailak University, Nakhon Si Thammarat, 80160, Thailand.

[c] School of Biomolecular Science and Engineering, Vidyasirimedhi Institute of Science and Technology (VISTEC), Wangchan Valley, Rayong 21210, Thailand

[d] Institute of Biochemistry, Department of Biotechnology and Enzyme Catalysis, Greifswald University, Felix-Hausdorff-Strasse 4, 17487 Greifswald, Germany

[e] Technical University of Berlin, Institute of Chemistry, Straße des 17. Juni 135, Sekr. L1, 10623 Berlin, Germany

Table of contents

I. Enzymes expression and purification

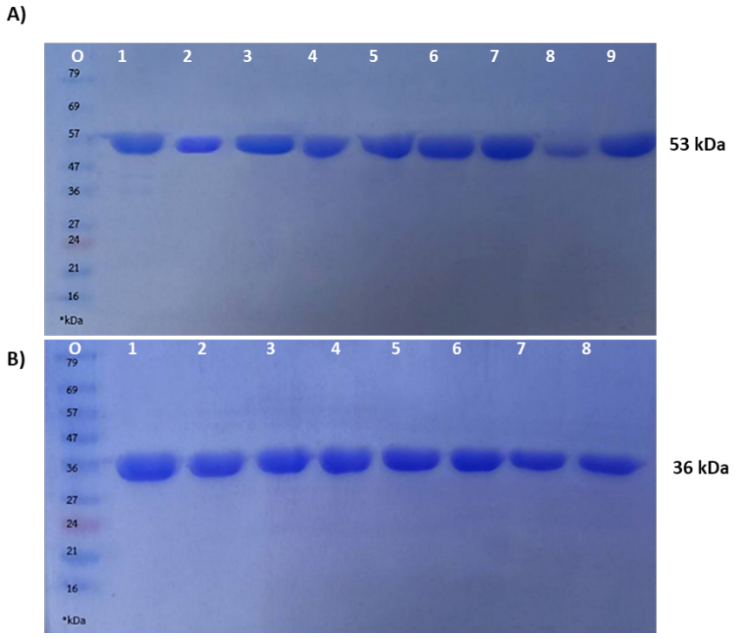

Fig S1. SDS-PAGE analysis of transaminases. A) 12 % SDS-PAGE analysis of purified (*S*)-selective transaminases. Lane 0: molecular weight markers, Lane 1: purified *Cvi*-TA (WT) (53 kDa), Lane 2: purified F88Y variant, Lane 3: purified F88Q variant, Lane 4: purified R416N variant, Lane 5: purified R416A variant, Lane 6: purified R416K variant, Lane 7: purified K288A variant, Lane 8: purified TA-10 (WT) (49 kDa), Lane 9: purified 3HMU-TA (WT) (51 kDa). B) 12 % SDS-PAGE analysis of purified (*R*)-selective transaminases. Lane 0: molecular weight markers, Lane 1: purified *Asp*-TA (WT) (37 kDa), Lane 2: purified Y58A variant, Lane 3: purified K179A variant, Lane 4: purified W183A variant, Lane 5: purified T273A variant, Lane 6: purified R126A variant, Lane 7: purified F113Y variant, Lane 8: purified F113Q variant. Molecular weights of transaminases were calculated from expasy.org.

II. Screening for transaminases

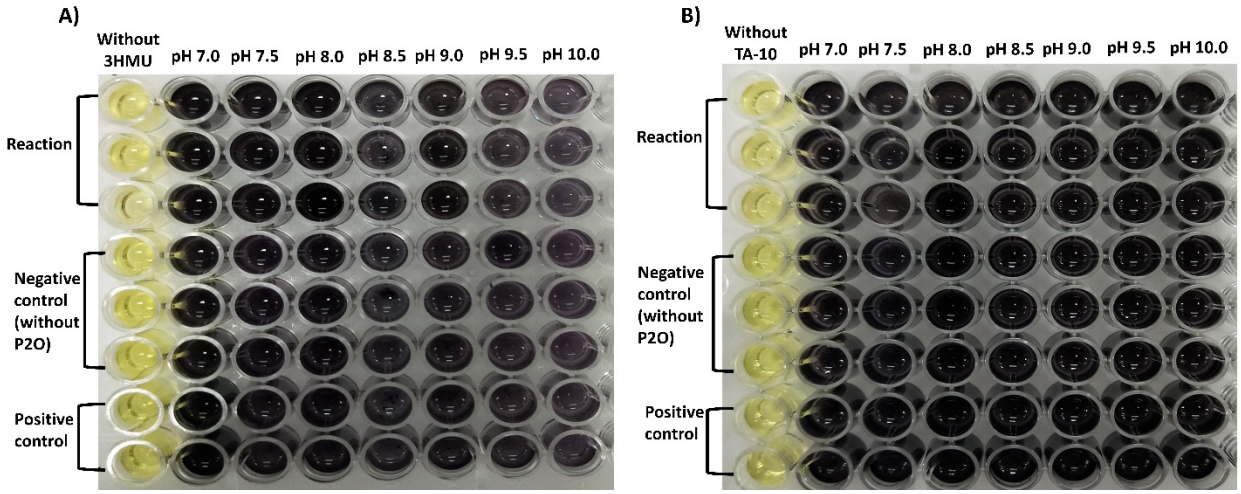

Fig. S2 Formation of dark precipitation indicating desired transaminase activities. The reactions of 3HMU-TA (A) and (B) TA10 and 2-keto-glucose were incubated at 30 °C in a shaker incubator at 220 rpm overnight.

The results of HTS using the diamine assay, which included also the (*S*)-selective transaminases 3HMU and TA10, indicated that the negative control reactions for both transaminases containing a sugar substrate and transaminase (without P2O) produced more dark precipitation compared to the negative control reaction of *Cvi*-TA (Fig 2A in the main text). Therefore, only *Cvi*-TA and *Asp*-TA were used as candidate enzymes for further study of mannosamine and galactosamine synthesis. The results of the second screening in one-pot synthesis using LC-MS/MS detection showed that mannosamine and galactosamine were formed in *Asp*-TA and *Cvi*-TA reactions, respectively. (Fig S3).

III. Tunnel Analysis and Molecular Docking

a. Tunnels and Molecular Docking in *Asp*-TA

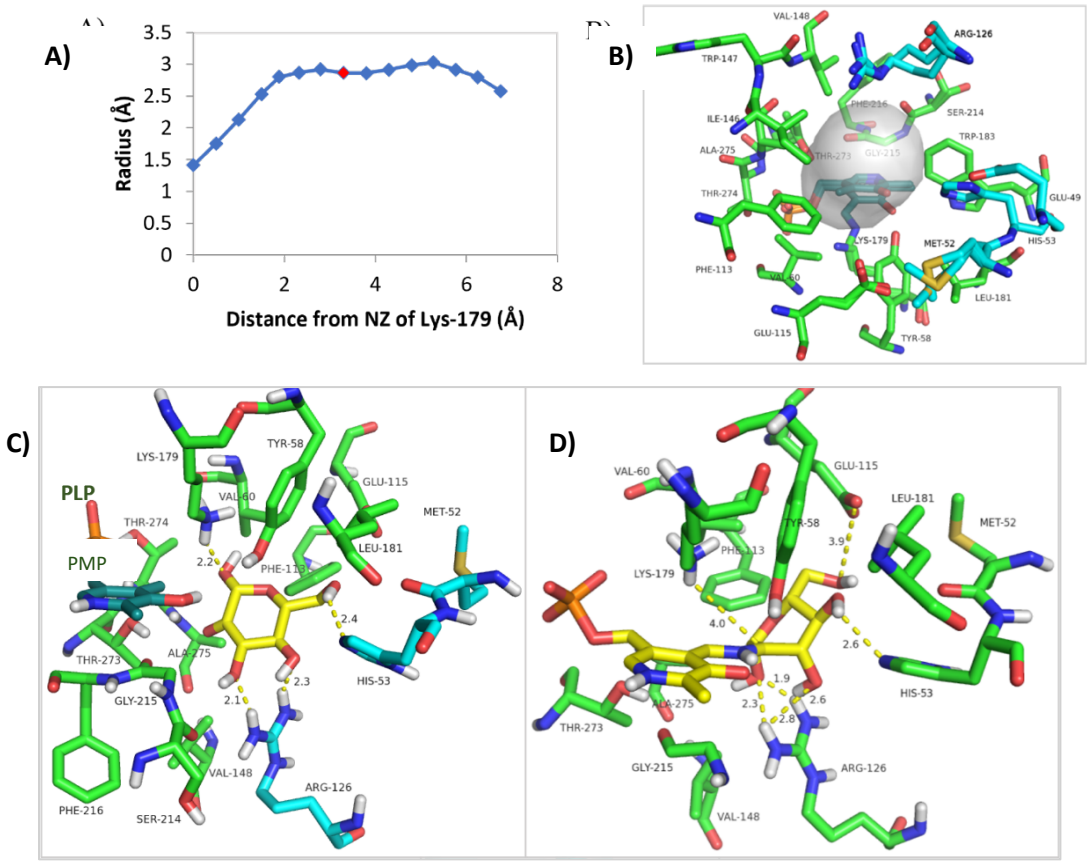

Fig. S3 Tunnel and Molecular Docking in *Asp*-TA. A) Plot indicating the radius and distance of a tunnel in *Asp*-TA with 2-keto glucose. The red point was chosen as the center of the docking box. B) The main tunnel in *Asp*-TA is shown in transparent surface and residues within 3 Å from the tunnel are shown. Chain A and B are shown in green and blue, respectively with PMP (dark green) binding. Residues within 3 Å of the tunnel are from both chain A (Tyr-58, Val-60, Phe-113, Glu-115, Ile-146, Trp-147, Val-148, Lys-179, Leu-181, Trp-183, Ser-214, Gly-215, Phe-216, Thr-273, Thr-274, Ala-275, and PLP) and Chain B (Glu-49, Met-52, His-53, and Arg-216). The binding mode of 2-keto-glucose (yellow) (C) and planar quinonoid (D) in *Asp*-TA. Residues within 5 Å from 2-keto-glucose and planar quinonoid are shown. Chain A and B are shown in green and blue, respectively.

Results from the CAVER Analyst identified a tunnel generated for 2-keto-glucose binding to *Asp*-TA. The plot illustrating the distance and radius of the tunnel relevant to 2-keto-glucose binding is shown in Fig. S4A. The residues within 3 Å of *Asp*-TA tunnel are from both Chain A and Chain B (Fig. S4B). Molecular docking of 2-keto-glucose in *Asp*-TA suggested that PMP could attack the *re* face of 2-keto-glucose to form the corresponding planar quinonoid (Fig. S3C). K179 donates a hydrogen bond (2.2 Å) to O1 of sugar. R126 donates two hydrogen bonds (2.1 and 2.3 Å, respectively) to O3 and O4 of the sugar. H53 accepts a hydrogen bond (2.4 Å) from O6 of the sugar. For 2-keto-galactose, O4 remains at the axial position. We proposed that O4 could interact with R126 or H53.

Molecular docking of the planar quinonoid in *Asp*-TA showed that the docked planar quinonoid overlapped with PLP in the crystal structure (Fig. S4D). The sugar moiety of the planar quinonoid is stabilized by hydrogen bonds. R126 donates hydrogen bonds to both O1 (2.3 and 1.9 Å) and O3 (2.8 and 2.6 Å) of the sugar moiety. H53 accepts a hydrogen bond (2.6 Å) from O4 of the sugar moiety. E115 accepts a hydrogen bond (3.9 Å) from O6 of sugar moiety. For the structure of the planar quinonoid of 2-keto-galactose-PMP complex, the O4 remains at the axial position. We proposed that O4 could interact with H53 or E115.

This study proposed that K179 could only donate a proton to the top face of the prochiral imine (4.0 Å). The proton can be donated to the equatorial position. Thus, the axial amino sugar can be formed in *Asp*-TA, suggesting that *Asp*-TA prefers to catalyze axial transamination reaction.

b. Tunnels and Molecular Docking in *Cvi*-TA

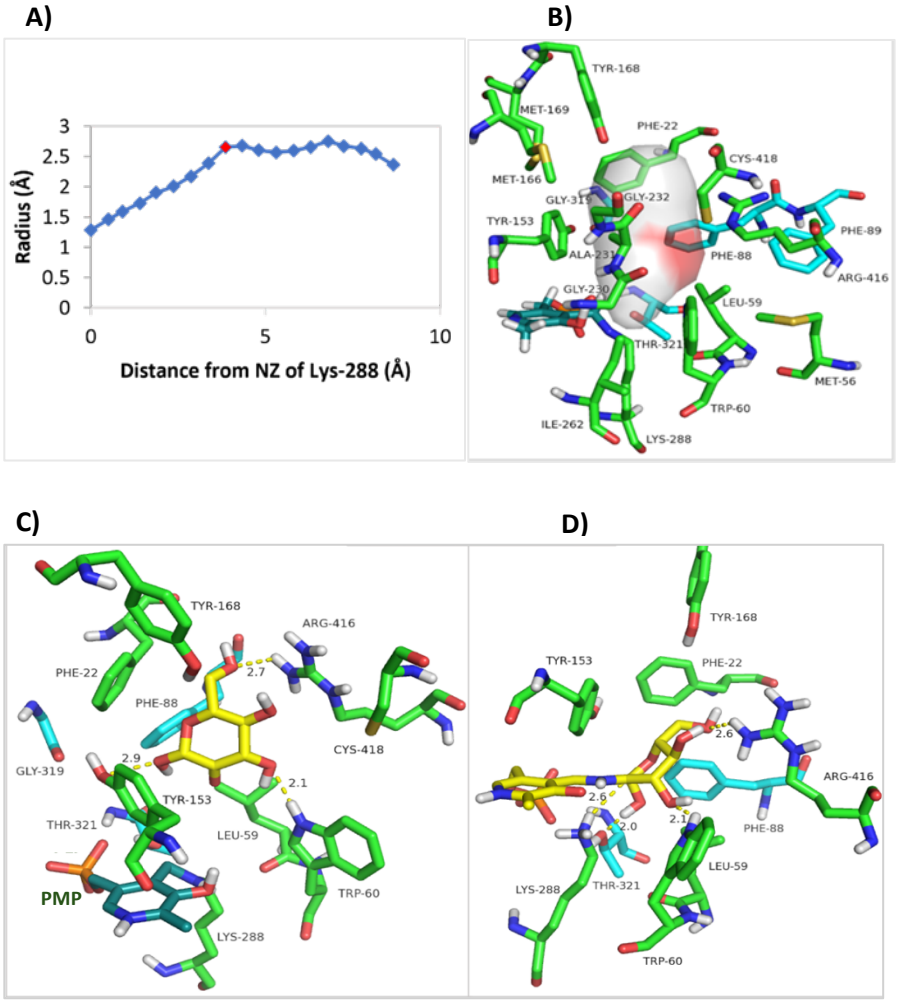

Fig.S4 Tunnel and Molecular Docking in *Cvi*-TA. A) Plot indicating the radius and distance of a tunnel in *Cvi*-TA with 2-keto glucose. The red point was chosen as the center of the docking box. B) The main tunnel in *Cvi*-TA is shown in transparent surface and residues within 3 Å from the tunnel are shown. Chain A and B are green and blue, respectively with PMP (dark green) binding. Residues within 3 Å of tunnel are from both Chain A (Phe-22, Met-56, Leu-59, Trp-60, Tyr-153, Met-166, Tyr-168, Met-169, Gly-230, Ala-231, Gly-232, Ile-262. Lys-288, Arg-416, Cys-418, and PLP) and Chain B (Phe-88, Phe-89, Gly-319, and Thr-321). The binding mode of 2-keto-glucose (yellow) (C) and planar quinonoid (D) in *Cvi*-TA. Residues within 5 Å from 2-keto-glucose and planar quinonoid are shown. Chain A and B are green and blue, respectively.

The results of the CAVER Analyst identified tunnels in *Cvi*-TA (Fig. S5) which is relevant to 2-keto-glucose binding (shown in Fig. S5A). The residues within 3 Å of *Cvi*-TA tunnels are from Chain A and Chain B (Fig. S5B). Molecular docking of 2-keto-glucose in *Cvi*-TA resulted in nine binding

modes. We selected the 2-keto-glucose binding mode shown in Fig. S5C because in this mode, PMP could attack the *re*-face of 2-keto-glucose to form the corresponding planar quinonoid. Y153 accepts a hydrogen bond (2.9 Å) from O1 of sugar. W60 donates a hydrogen bond (2.1 Å) to O3 of sugar. R416 interacts with O4 and O6 (2.7 Å) of sugar. For 2-keto-galactose, O4 remains at the axial position. We proposed that O4 could interact with R416.

Molecular docking of a planar quinonoid in *Cvi*-TA resulted in twenty binding modes. We selected the mode shown in Fig. S5D because the docked planar quinonoid is overlapped with PLP in the crystal structure. The sugar moiety of the planar quinonoid is stabilized by hydrogen bonds (Figure S5D). T321 accepts a hydrogen bond (2.0 Å) from O1 of sugar moiety. W60 donates a hydrogen bond (2.1 Å) to O3 of sugar moiety. R416 interacts with O4 and O6 (2.6 Å) of the sugar moiety. For the structure of the planar quinonoid of 2-keto-galactose-PMP complex, O4 remains at the axial position. We proposed that O4 could interact with R416.

Our analysis proposed that K288 could only donate a proton to the bottom face of the pro-chiral imine (2.6 Å). The proton is donated to the axial position. Thus, the equatorial amino sugar can be formed in *Cvi*-TA, suggesting that *Cvi*-TA can catalyze equatorial transamination reaction.

Table S1. Location of residues around the 2-keto-glucose and planar quinonoid binding sites in *Asp*-TA

Residues	located close to 2-keto-glucose	located close to planar quinonoid
Y58	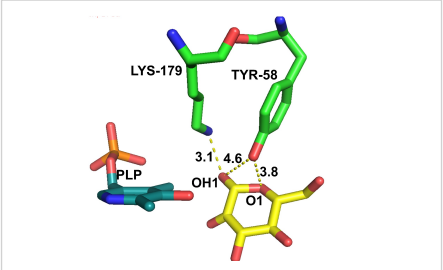	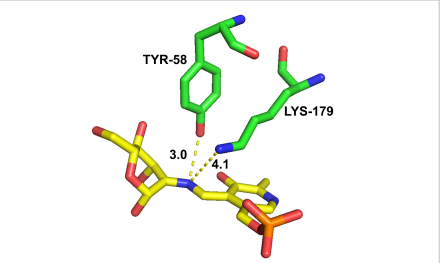
T273	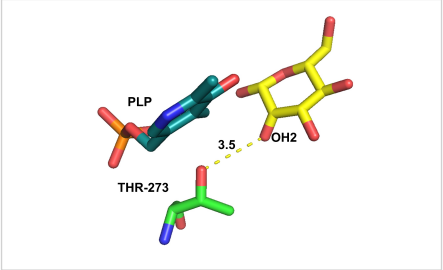	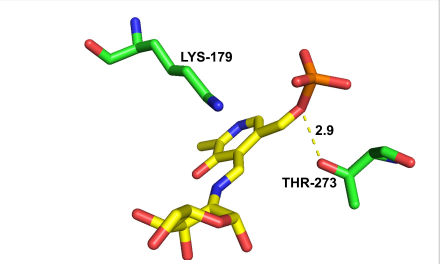
R126	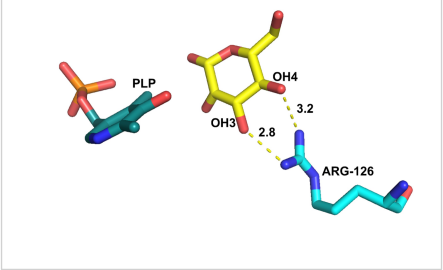	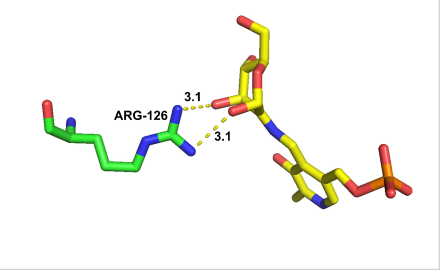
F113	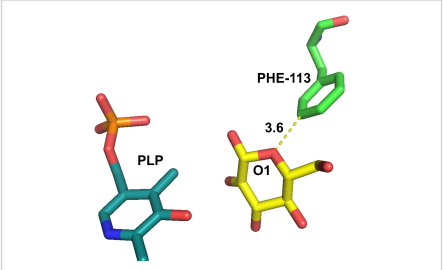	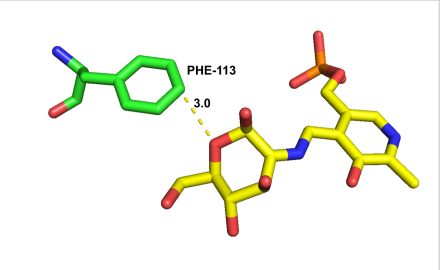

Residues	located close to 2-keto-glucose	located close to planar quinonoid
W183	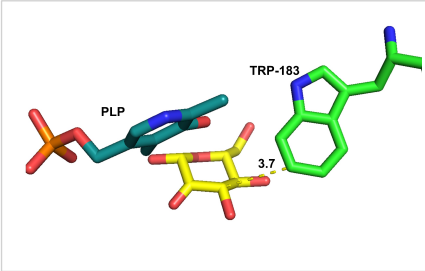	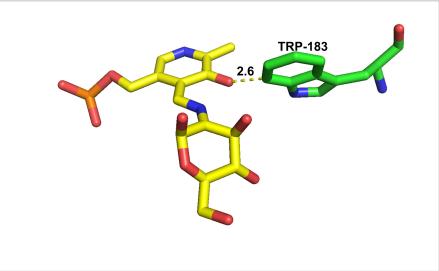

Table S2. Location of residues around the 2-keto-glucose and planar quinonoid binding sites in *Cvi*-TA

Residues	located close to 2-keto-glucose	located close to planar quinonoid
R416	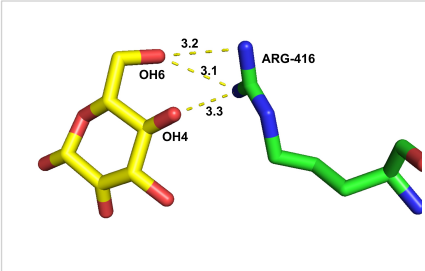	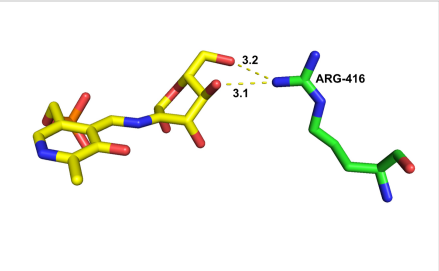
K288	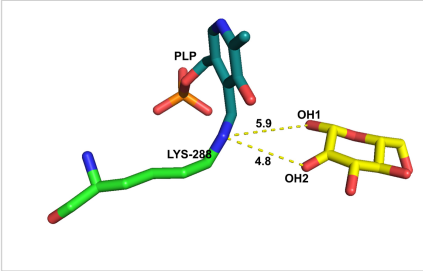	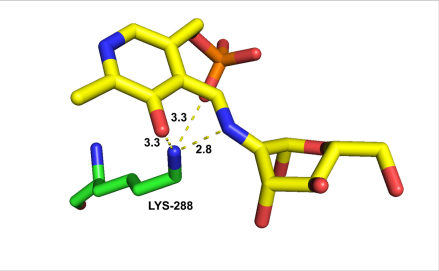

Residues	located close to 2-keto-glucose	located close to planar quinonoid
F88	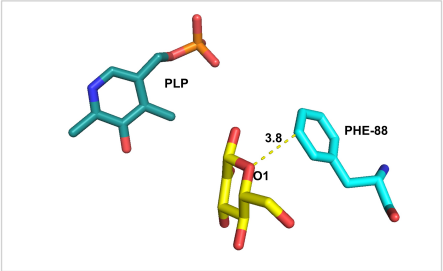	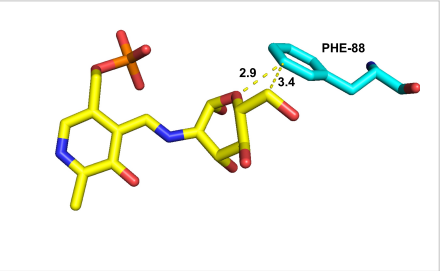

IV. Enzyme engineering by site-directed mutagenesis

Table S3. Primers designed for the site-directed mutagenesis of *Cvi*-TA and *Asp*-TA.

Primers	Sequences (5'→3')
F_R416A_*Cvi*	CAATAATCTGATTATG**GCA**GCCTGTGGTG
R_R416A_*Cvi*	CACCACAGGC**TGC**CATAATCAGATTATTG
F_R416K_*Cvi*	CAATAATCTGATTATG**AAA**GCCTGTGGTG
R_R416K_*Cvi*	CACCACAGGC**TTT**CATAATCAGATTATTG
F_R416N_*Cvi*	CAATAATCTG**ATT**ATGAATGCCTGTGGTG
R_R416N_*Cvi*	CACCACAG**GCA**TTCATAATCAGATTATTG
F_K288A_*Cvi*	GTTTACCGCAGCC**GCA**GGCTTATCTTCT
R_K288A_*Cvi*	AGAAGATAAGCC**TGC**GGCTGCGGTAAAC
F_ F88Q_*Cvi*	GCCGTTTTATAATACC**CAG**TTTAAAACCACCC
R_ F88Q_*Cvi*	GGGTGGTTTTAAA**CTG**GGTATTATAAAACGGC
F_ F88Y_*Cvi*	GCCGTTTTATAATACC**TAT**TTTAAAACCACCC
R_ F88Y_*Cvi*	GGGTGGTTTTAAA**ATA**GGTATTATAAAACGGC
F_Y58A_*Asp*	GTGATCTGACC**GCG**GATGTTATTAGCG
R_Y58A_*Asp*	CGCTAATAACATC**CGC**GGTCAGATCAC
F_K179A_*Asp*	CATTTGATCCGACCATT**GCA**AACCTGCAGTG
R_K179A_*Asp*	CACTGCAGGTT**TGC**AATGGTCGGATCAAATG
F_W183A_*Asp*	CATTAAAAACCT**GCA**GGCAGGTGATCTGAC
R_W183A_*Asp*	GTCAGATCACC**TGC**CTGCAGGTTTTTAATG

Primers	Sequences (5'→3')
F_T273A_*Asp*	GAAATTTTTATGTGT**GCA**ACGGCCGGCG
R_T273A_*Asp*	CGCCGGCCGT**TGC**ACACATAAAAATTTC
F_R126A_*Asp*	GACCGGTGTT**GCA**GGTTCTAAAC
R_R126A_*Asp*	GTTTAGAACC**TGC**AACACCGGTC
F_F113Q_*Asp*	GCATTCGTGATGCG**CAG**GTGGAAGTTATTG
R_ F113Q_*Asp*	CAATAACTTCCAC**CTG**CGCATCACGAATGC
F_ F113Y_*Asp*	GCATTCGTGATGCG**TAT**GTGGAAGTTATTG
R_F113Y_*Asp*	CAATAACTTCCAC**ATA**CGCATCACGAATGC

V. Mannosamine and galactosamine synthesis utilizing P2O and transaminase

a. Reaction optimization for amino sugars synthesis

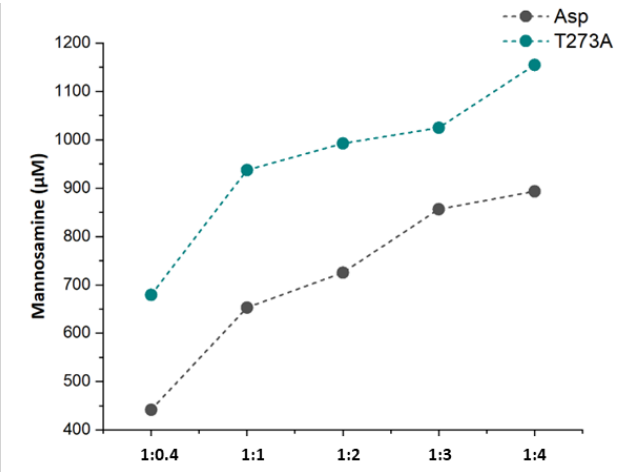

Fig. S5 Amount of mannosamine formed at various ratios of glucose: (*R*)-PEA concentrations in the reaction of T273A (green line) variant compared to those of *Asp*-TA (gray line).

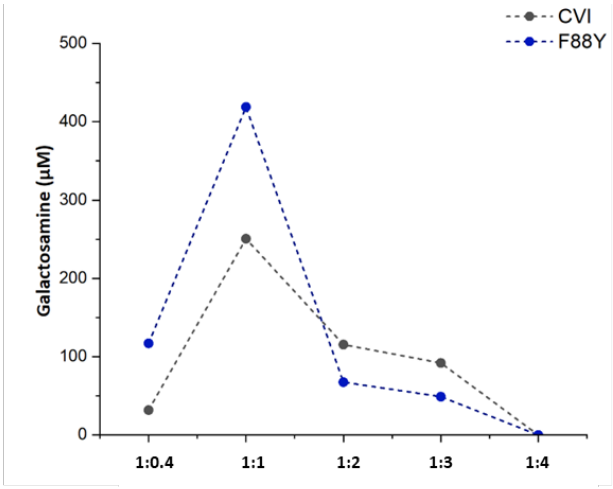

Fig. S6 Amount of galactosamine formed at various ratios of galactose: *S*-PEA concentrations in the reaction of the F88Y (blue line) variant compared to that of *Cvi*-TA (gray line).

b. Amino sugars synthesis *via* one-pot reaction of engineered P2O and transaminase

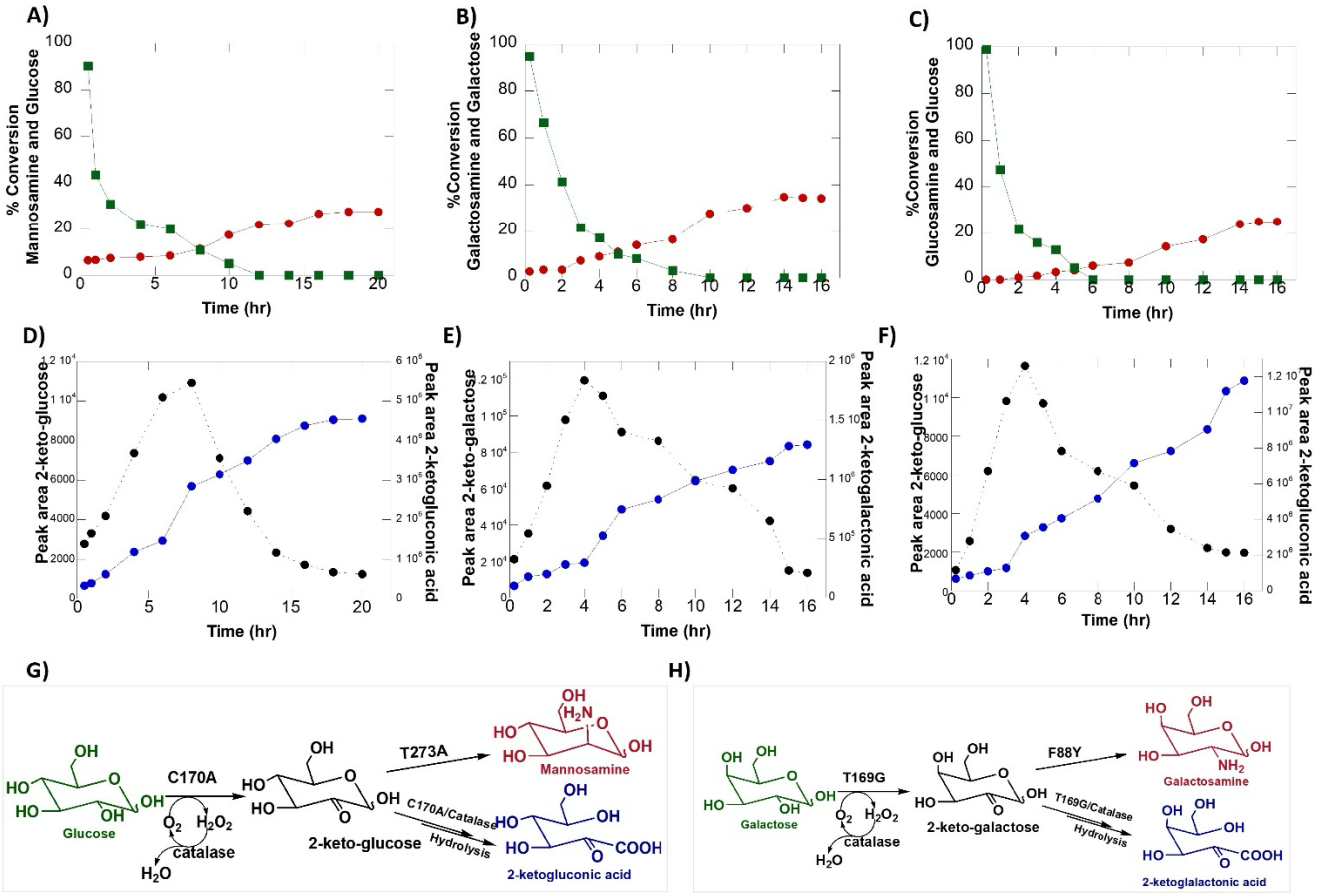

Fig. S7 Amino sugars synthesis *via* one-pot reaction of engineered P2O and transaminase. Mannosamine (A), galactosamine (B) and glucosamine (C) synthesized from multiple turnovers of P2O and transaminase variants. Percentage of sugar substrate conversion is shown as green squares while red circles represent the percentage of amino sugars formed. D- F) Peak areas of 2-keto-sugars intermediate formation are shown as black circles while those of sugar acid formation are shown as blue circles. The proposed mechanism of mannosamine (G) and galactosamine (H) synthesis from multiple turnovers of P2O and transaminase.

VI. LC-MS/MS analyses

Table S4. MS Conditions for measurement of relevant compounds in mannosamine and galactosamine synthesis

Compounds	Precursor ion (m/z)	Product ion (m/z)	Transition for MRM condition	Collision energy (eV)	Mode
Glucose	179	59, 89	179:89	3	Negative
Galactose	179	59, 89	179:89	2	Negative
Mannosamine	180	59, 72	180:72	15	Positive
Galactosamine	180	59, 72	180:72	15	Positive
Glucosamine	180	59, 72	180:72	15	Positive
2-keto-glucose	177	89 ,99, 117	177:99	8	Negative
2-keto-galatose	177	89, 99, 117	177:99	8	Negative
2-keto-gluconic acid	193	-	-	-	Negative
2-keto-galactonic acid	193	-	-	-	Negative

Product analysis of one-pot, multiple turnover reactions of engineered P2O and transaminase by LC-MS/MS

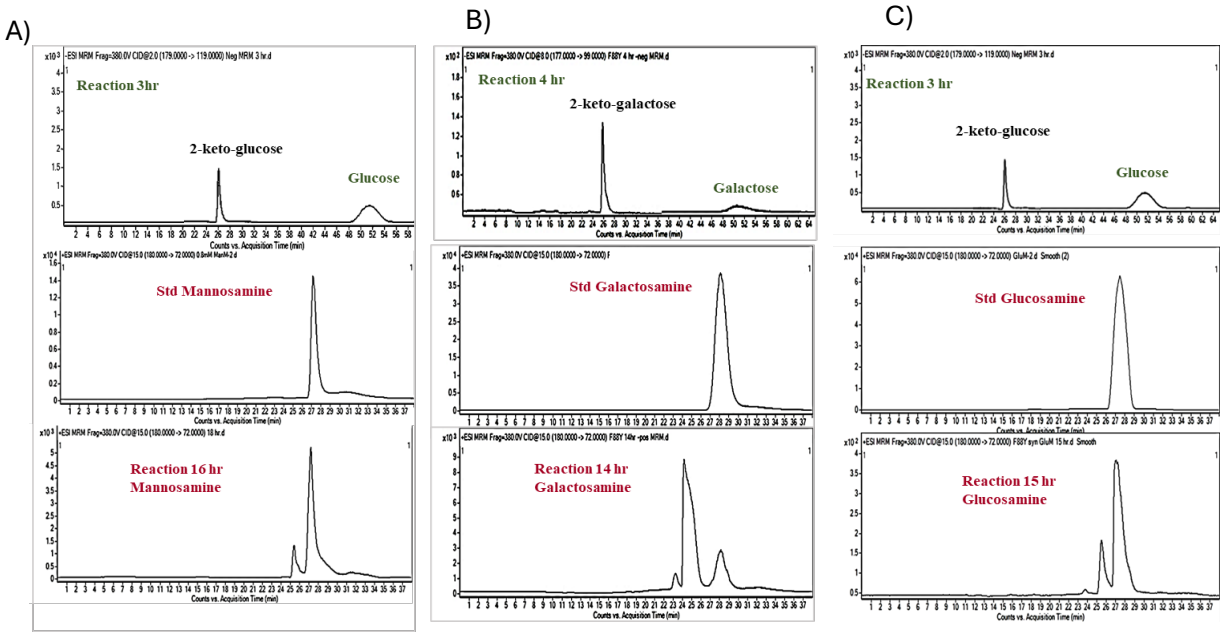

Figure S8. Product analysis of one-pot, multiple turnover reactions of engineered P2O and transaminase by LC-MS/MS. A) Product analysis of multiple turnover reactions of P2O (C170A) and *Asp*-TA (T273A) to convert D-glucose to mannosamine by LC-MS/MS analysis. Total ion chromatograms show depletion of glucose (eluted at 51 min, transition 179:119 m/z) and formation of 2-keto-glucose (eluted at 26 min, transition 177:99 m/z) and mannosamine (eluted at 27 min, transition 180:72 m/z) over time. Standard mannosamine (eluted at 27 min, transition 180:72 m/z) are shown as references. B) Product analysis of multiple turnover reactions of P2O (T169G) and *Cvi*-TA (F88Y) to convert galactose to galactosamine by LC-MS/MS analysis. Total ion chromatograms show depletion of galactose (eluted at 51 min, transition 179:119 m/z) and formation of 2-keto-galactose (eluted at 26 min, transition 177:99 m/z) and galactosamine (eluted at 28 min, transition 180:72 m/z) over time. Standard galactosamine (eluted at 28 min, transition 180:72 m/z) are shown as references. C) Product analysis of multiple turnover reactions of P2O (C170A) and *Cvi*-TA (F88Y) to convert glucose to glucosamine by LC-MS/MS analysis. Total ion chromatograms show depletion of glucose (eluted at 51 min, transition 179:119 m/z) and formation of 2-keto-glucose (eluted at 26 min, transition 177:99 m/z) and glucosamine (eluted at 27 min, transition 180:72 m/z) over time. Standard glucosamine (eluted at 27 min, transition 180:72 m/z) are shown as references.

Sugar acid formation from multiple turnover reactions of engineered P2O and transaminase

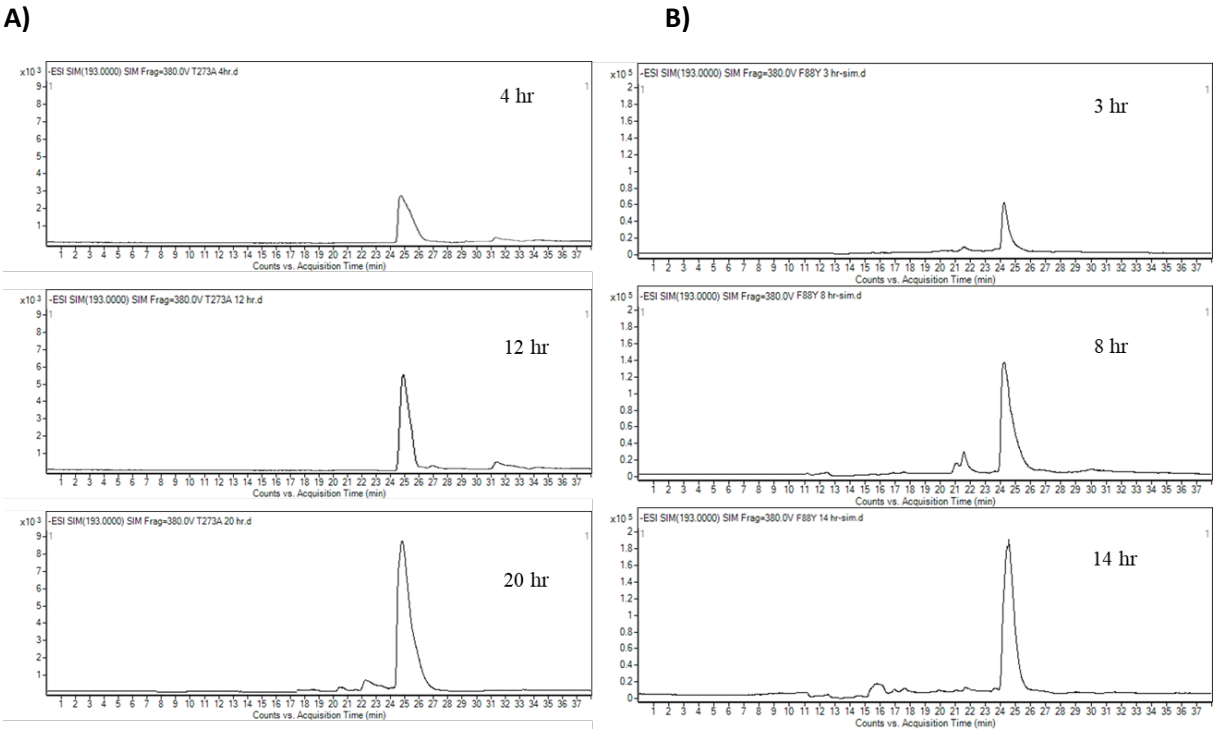

Figure S9. Sugar acid formation from multiple turnover reactions of engineered P2O and transaminase**.** Total ion chromatograms show formation of sugar acid (193 m/z) at various time points of multiple turnovers of P2O and transaminases. A) Formation of 2-ketogluconic acid eluted at 25 min. B) Formation of 2-ketogalactonic acid eluted at 24.5 min.

VIII. Analytical results of 9-fluorenylmethoxycarbonyl-galactosamine

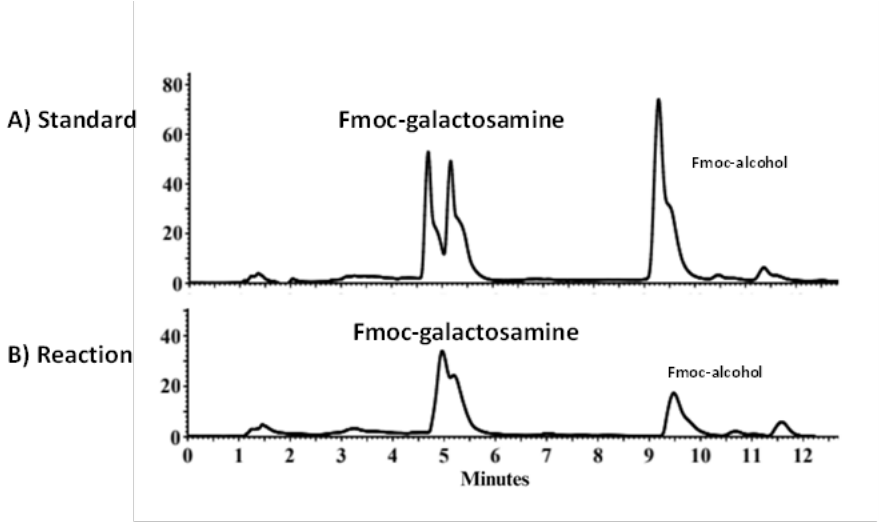

Figure S10. HPLC chromatogram of Fmoc-galactosamine. Fmoc-galactosamine analyzed was from (A) derivatization of standard galactosamine and (B) derivatization of galactosamine from the reaction of engineered P2O and transaminase

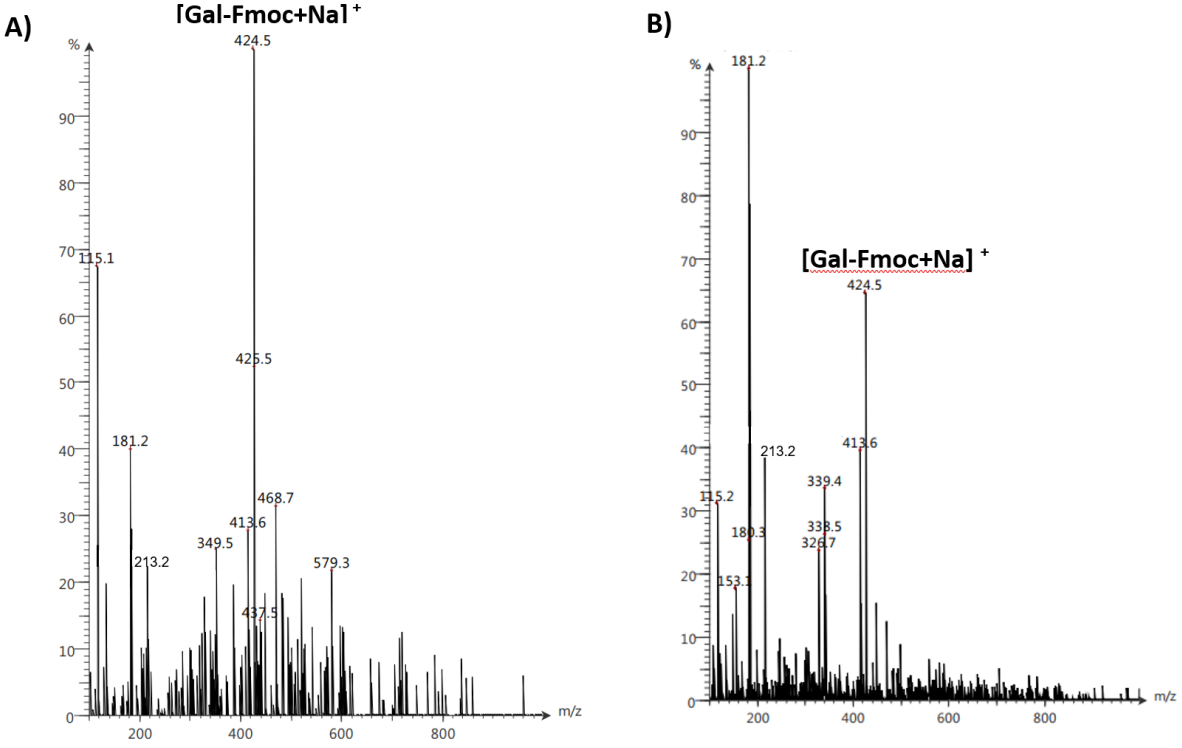

Figure S11. Mass spectra of Fmoc-galactosamine. A) The mass spectrum of purified Fmoc-galactosamine from the reaction of engineered P2O and transaminase shows the formation of

$[M+Na]^+$ at 424.5 m/z. B) This peak was also found in a mass spectrum of Fmoc-galactosamine obtained from the reaction of the standard galactosamine.